ASTR-3415: Astrophysics Course Lecture Notes Section VII

Dr. Donald G. Luttermoser
East Tennessee State University

Spring 2003
Version 1.2

Abstract

These class notes are designed for use of the instructor and students of the course ASTR-3415: Astrophysics. This is the Version 1.2 edition of these notes.

VII. Stellar Evolution: Old Age and Death

A. Post Red Giant Evolution.

1. Red Giant Clump stars (Pop. I) and Horizontal Branch stars (Pop. II) are *helium-core burners* (they also are undergoing H-shell burning). Approximately 10% of a star's nuclear burning lifetime is spent in this stage.

2. The path a star takes on its road to stellar death depends upon its initial mass and the amount of mass loss suffered during the AGB phase (see below) of its life. Note that the following masses correspond to the mass of the star when it was on the main sequence. The boundary masses for some of these various regimes are somewhat uncertain. When possible, I'll use the values from the textbook unless they contradict those values from recent calculations. Once again, I will just go over the highlights here. Your textbook (*i.e.*, Carroll and Ostlie) go into quite a bit more detail, so make sure you read Chapter 13 in depth.

3. $\boldsymbol{M < 0.08 M_\odot}$: These objects never ignite hydrogen and hence never become main sequence stars. These objects are called **brown dwarfs**. They are bright at infrared wavelengths from energy liberated from contraction.

4. $\boldsymbol{0.08 M_\odot < M \lesssim 0.4 M_\odot}$: These stars are totally convective, and as such, helium ash gets uniformly mixed throughout the star. No inert helium core develops, hence no H-shell burning and no expansion into a red giant. After hydrogen is exhausted, the entire star contracts until the helium becomes degenerate

(see the white dwarf section, §VIII.A) and the star becomes a **helium-rich white dwarf**.

5. **$0.4M_\odot \lesssim M \lesssim 4M_\odot$**: These stars ignite helium in a degenerate core (*i.e.*, the He-core flash, see §VI.C.2.h on page VI-12 of the course notes). During the core He-fusion stage, the star sits in the red giant *clump* (Population I stars) or the horizontal branch (Population II stars) on the H-R Diagram. He-fusion creates ^{12}C and ^{16}O ash and once the He-fusion stops, the carbon-oxygen core continues to collapse.

   a) This causes energy to be dumped into the He-rich layer just above the core which ignites $\Longrightarrow$ the star now has a He-burning shell and H-burning shell (see Fig. 13.8 on page 501 in the textbook). This extra energy source expands the outer layers of the star further — the star becomes a bit more red and a lot more luminous.

   b) During this time, the star moves up the **asymptotic giant branch** (AGB) on the H-R Diagram $\Longrightarrow$ the path on the H-R Diagram is *asymptotic* to the red giant branch.

   c) The outer layers of the star can become unstable during this phase and it can begin to pulsate $\Longrightarrow$ **long period variable** (see §VII.B).

   d) A variety of things are occurring in the interior shells just above the collapsing C-O core.

      i) As the He-burning shell uses up its fuel, it gets thinner and thinner.

      ii) At the same time, the H-burning shell above the He-burner shell continuously dumps additional He onto the He-burning shell.

Figure VII–1: Power output of thermal pulses of an AGB star.

iii) As the He-burning shell thins (at the bottom of the He-rich internal shell), the density of the gas continuously increases due to the added He settling from the H-burning shell above.

iv) This cause the He-burning shell to become slightly degenerate and unstable $\Longrightarrow$ this shell experiences what are called thermal relaxation oscillations.

v) The shell goes through a series of **thermal pulses** (see Fig. VII-1 of these notes and Fig. 13.9 of the textbook) which are also called **He-shell flashes**.

vi) During a thermal pulse, the luminosity of the star increases for a short time (approximately 100 years). Also, the surface pulsations can change

their periods during this time as well. *R Hya* is a long period variable that has just gone through such a thermal pulse.

e) While this is going on, the interior of the star also experiences *dredge-ups*:

i) A "dredge-up" simply means that nuclear processed material is being brought from the interior of the star up into the stellar atmosphere where it can be detected in the emergent spectrum of the star.

ii) The **first dredge-up** occurs when the surface convection zone dips down far enough to start interacting with the H-burning shell's upper layers while the star is on the **red giant branch**.

- Remember, this initial H-shell burning involves the CNO cycle and causes the star to expand up to the red giant regime on the H-R Diagram.

- The cooler upper layers of this H-burning shell are only carrying out (predominantly) the first two steps of the CNO cycle.

- As such, enhanced levels of ^{13}C with respect to ^{12}C are brought to the star's photosphere $\Longrightarrow$ if the $^{13}C/^{12}C$ ratio exceeds solar values, we know that RGB star has gone through this star of evolution.

iii) As an AGB star expands its outer envelope, the effective temperature of star drops which causes the convection zone to deepen until it begins to reach below the H-burning shell to the He-rich layer below it (though not quite to the He-burning shell — see Fig. 13.8 on page 501 in the textbook). This results in the **second dredge-up** which enhances both the helium (from the He-rich layers) and nitrogen abundance (from the CNO cycle in the layers above these He-rich layers).

iv) Each thermal pulse increases the energy flux from the He-burning shell. For stars with $M \gtrsim 2.0$ $M_\odot$, this results in the formation of a convection zone between the He-burning shell and the H-burning shell above. As a result, the AGB star's surface convection now extends all of the way down to the He-burning shell.

v) For these $2M_\odot$ and above AGB stars, carbon produced in the He-burning shell finds its way to the surface through deep convection cells $\Longrightarrow$ the star becomes either an S star (with C/O ~ 1.0) or a carbon (R or N) star (with C/O > 1.0). *TX Psc* is an example of a carbon star that has already gone through a series of thermal pulses.

f) Strong stellar winds begin as the star goes up the AGB due to the increased luminosity and the lower surface gravity, and hence escape velocity.

i) Pulsations also assist in lifting mass out of the potential well of the star.

ii) IR radiation pressure on molecular lines, though not strong enough to drive a stellar wind, also helps to lift the gas out of the potential well of the star (see Jørgensen & Johnson 1992, *Astron. & Astrophys.*, 265, 168).

iii) Dust starts to form in earnest in the uppermost layers of these stars and the large IR flux imparts a net momentum outward. The dust hits the gas on the way out which drives the gas off too.

iv) During this phase, mass-loss rates can reach as high as $10^{-4} M_\odot$/yr.

v) In time, the envelope of the star detaches from the core. This phase is often referred to as the **superwind** epoch which results in the formation of **OH/IR sources**.

- These objects appear to be stars shrouded in optically thick dust clouds that radiate their energy primarily in the infrared.

- The OH part of the OH/IR designation is due to the emission of OH maser (**m**icrowave **a**mplification by **s**timulated **e**mission of **r**adiation) emission.

vi) The material above the collapsing core continues to move away and at this point is called a **pre-planetary nebula** star.

vii) Finally, the shell becomes optically thin to the radiation (composed primarily of X-ray, EUV, UV, and visible light) from the hot collapsing core. The UV/EUV/X-ray photon flux fluoresces and ionizes the surrounding shell, now over a light year across, which is seen as a **planetary nebula**.

viii) In time, the planetary nebula's density gets so thin that the H-Balmer line and [O III] emission line flux gets too weak to be seen $\Longrightarrow$ the planetary nebula disappears.

ix) The envelope of the star merges with the surrounding interstellar medium (which enriches the ISM with its nuclear processed material) and all that is left is the cooling, collapsing core of the star.

g) The structure and spectrum of a planetary nebula is determined from the density and incident radiation from the stellar core falling on the inner side of the expanding shell. Typically spherical symmetry is assumed for the shell, however observations reveal many planetaries that are not spherically symmetric.

i) We assume here that all radiative and collisional processes going on in the nebula operate on time scales that are short relative to the time required for large–scale changes in the structure of the nebula $\Longrightarrow$ a *steady state* model.

ii) The radiation intensity I_ν at point r in the nebula consists of 2 parts:

$$I_\nu = I_\nu^s + I_\nu^d, \tag{VII-1}$$

where I_ν^s corresponds to the stellar component (*i.e.*, light from the collapsing core) and I_ν^d is the diffuse term due to photons created by the nebula itself.

iii) The stellar component of the radiation field can be determined from

$$4\pi\, J_\nu^s = 2\pi \int_{-1}^{1} I_\nu^s\, d\mu = \frac{R^2}{r^2}\,\pi F_\nu = \frac{L_\nu(r)}{4\pi\, r^2}, \tag{VII-2}$$

where $L_\nu(r)$ is the monochromatic luminosity [ergs /cm^2/s/Hz/sr] of the star at distance r from the core, J_ν^s is the mean intensity of the core's light at this distance, and πF_ν is the flux at the surface of the core.

iv) The transfer equations for the terms is Eq. (VII-1) are

$$\frac{dL_\nu(r)}{dr} = -\kappa_\nu\, L_\nu(r), \tag{VII-3}$$

$$\frac{dI_\nu^s}{ds} = -\kappa_\nu\, I_\nu^d + \epsilon_\nu\ , \tag{VII-4}$$

which can be compared to the equation of radiative transfer given in Eqs. (I-21) and (I-22) in §I of the notes.

- The opacity κ_ν, here, will be given by

$$\begin{aligned} \kappa_\nu &= \sum_i n_i\, \alpha_\nu(i) \qquad\qquad (\text{VII-5}) \\ &\simeq n_1(\mathrm{H}^0)\, \alpha_{1,\nu}(\mathrm{H}^0) + n_1(\mathrm{He}^0)\, \alpha_{1,\nu}(\mathrm{He}^0)\ , \end{aligned}$$

where $n_1(\mathrm{H}^0)$ and $n_1(\mathrm{He}^0)$ are the number densities [cm^{-3}] in the ground state of neutral hydrogen and neutral helium, respectively, and $\alpha_{1,\nu}(\mathrm{H}^0)$ and $\alpha_{1,\nu}(\mathrm{He}^0)$ are the absorption coefficients [cm^2] or *cross-sections* of the bound-free transitions from the ground state of these two species (see Eq. I-25). In general, the sum should be over all ions or atoms that can be further ionized by the radiation source, but neutral hydrogen (H^0 = H I) and neutral helium (He^0 = He I) are the dominant sources that give rise to the opacity in the planetary nebula shell.

- The emissivity ϵ_ν describes the photons emitted from the gas, and does not include direct radiation from the ionizing star.

v) Ionization equilibrium exists in the planetary nebula shell, and as such, photoionization and recombination processes occur with equal rates. For $\mathrm{H}^0 + \gamma \rightleftharpoons \mathrm{H}^+ + \mathrm{e}^-$ (here H^+ = H II = proton), ionization equilibrium is obtained if

$$n_1(\mathrm{H}^0) \int_{\nu_1}^{\infty} \frac{4\pi J_\nu(r)}{h\nu} \alpha_{1,\nu}(\mathrm{H}^0) d\nu = n_e n(\mathrm{H}^+) \alpha_B(\mathrm{H}^0) = n_e n_p \alpha_B(\mathrm{H}^0) \qquad \text{(VII-6)}$$

- Here, $n(\mathrm{H}^+)$ is the number density of ionized hydrogen particles = number of protons n_p.

- α_B is called the *recombination coefficient* [cm^3/s] and can be interpolated from the values listed in Table VII-1.

Table VII–1: Recombination Coefficient for Hydrogen.

T (K)	5000	10,000	20,000
α_B (cm^3 s^{-1}	4.54×10^{-13}	2.60×10^{-13}	1.43×10^{-13}

- Eq. (VII-6) simply states that the number of ionizations per second equals the number of recombinations per second.

vi) Since the gas is in ionization equilibrium, the heating of the gas, Γ [ergs/cm^3/s], is due to the photoelectrons (and initially not to the photons themselves), which are emitted with an energy

$$\epsilon_e = \frac{1}{2} m_e v^2 = h\nu - \chi_k = h(\nu - \nu_k), \qquad \text{(VII-7)}$$

where χ_k is the ionization energy from the ground state of the k-th species.

vii) The rate at which the electrons heat the gas is given by the product of the flux of ionizing photons, the ionization cross section, the number density of neutral atoms, and the electron energy, integrated over frequency. For hydrogen

$$\begin{aligned} \Gamma &= n(\mathrm{H}^0) \int_{\nu_1}^{\infty} \frac{4\pi J_\nu(r)}{h\nu} \epsilon_e \alpha_\nu(\mathrm{H}^0)\, d\nu \qquad \text{(VII-8)} \\ &= n_e n_p \alpha_B(\mathrm{H}^0) h\overline{\nu}, \qquad \text{(VII-9)} \end{aligned}$$

where $h\overline{\nu}$ represents the average energy of the ionizing photons.

- For most nebula, $h\nu_1 \gg k_B T_{\rm eff}$, where $T_{\rm eff}$ is the effective temperature of the ionizing star (*i.e.*, collapsing core).

- If the local spectrum $J_\nu(r)$ is nearly Planckian, and there is little absorption, then $h\overline{\nu} \approx k_B T_{\rm eff}$ $\Longrightarrow$ thus $T_{\rm eff}$ can be thought of as the initial temperature of the medium before recombination and cooling are considered.

- We can determine this average photon energy $h\overline{\nu}$ from the luminosity of the star by solving Eq. (VII-2) in conjunction with Eqs. (VII-8) and (VII-9).

viii) Finally, the thermal state of the gas is determined by the energy equilibrium equation

$$\Gamma = \Lambda_c + \Lambda_{\rm ff} + \Lambda_R \ , \qquad \text{(VII-10)}$$

which states that the energy gain per unit volume per second Γ (*i.e.*, heating) of the gas is balanced by:

- The net energy loss [erg/cm^3/s] through the emission of photons in spectral lines after a collisional excitation,

$$\Lambda_c = \sum_k \sum_i n_{ki} \sum_{j>i} A_{ji} h\nu_{ji} \ , \qquad \text{(VII-11)}$$

where the k-index represents the *atomic species* to which the line belongs, i is the lower level, and j is the upper level of the bound-bound transition of all line transitions that are important in cooling the gas. Also, A_{ji} is the **Einstein A-value**, which is related the the oscillator strength of a transition and is equal to the reciprocal of the average time an electron stays in the excited state. Typically the most

important lines in radiative cooling are the forbidden lines of [O II] (doublet at 3726.0 Å and 3728.8 Å), [O III] (triplet at 4931.0 Å, 4958.9 Å, and 5006.9 Å), [N II] (triplet at 6527.1 Å, 6548.1 Å, and 6583.4 Å), and Hα (6562.8 Å) for temperatures above 6000 K, and [O III] (triplet at 32.7 μ, 51.8 μ, and 88.4 μ [$\mu \equiv$ micron $= 10^{-6}$ m]) for temperatures below this.

- Through thermal **bremsstrahlung** (or "braking radiation" $\equiv$ electrons that scatter off ions in the gas, which causes the electrons to emit photons),

$$\Lambda_{\rm ff} = 1.4 \times 10^{-27}\, g_{\rm ff} Z^2 T_e^{1/2} n_e n_{\rm ion} \ , \qquad \text{(VII-12)}$$

where Z is the integer charge ($Z = 1$ for hydrogen) of the ions at density $n_{\rm ion}$, n_e is the electron number density, and $g_{\rm ff}$ is the mean Gaunt factor for free-free emission. Typically, in nebular conditions, $1.0 < g_{\rm ff} < 1.5$ and one usually sets the Gaunt factor to an average value of 1.3. Since the ion density is going to be dominated by ionized hydrogen and singly-ionized helium in planetary nebulae, $n_{\rm ion} = n_p + n({\rm He}^+)$, both with $Z = 1$.

- Through radiative recombination,

$$\Lambda_R = n_p \sum_{n=2}^{\infty} \int_0^{\infty} n_e v \epsilon_e \sigma_n(v) f(v) dv \ , \qquad \text{(VII-13)}$$

where v is the velocity of the distribution of electrons $f(v)$, where $f(v)\, dv$ is given by the Maxwell-Boltzmann distribution (Eq. III-5). Also,

ϵ_e is given by Eq. (VII-7), and $\sigma_n(v)$ is the recombination cross-section of the transition. Figure VII-2 shows the various heating and cooling rates that are important in a planetary nebula.

ix) With the above describe equations, one can deduce detailed models of planetary nebula which can then be tested through observations of various emission lines that the nebula gives off. Certain lines ratios then give temperatures, electron densities, etc.

h) The contracting carbon-oxygen core becomes degenerate before carbon fusion can begin for stars in this mass range — the star is now dead (in a thermonuclear sense) as a **carbon-oxygen rich white dwarf**. Figure VII-3 summarizes the evolutionary path that a one-solar mass star (like the Sun) takes on the H-R Diagram.

6. $\boldsymbol{4M_\odot \lesssim M \lesssim 8M_\odot}$: These stars ignite ^{12}C in a degenerate core.

a) These stars follow the same AGB sequences as the lower mass stars up until the superwind phase of the lower mass stars. Before any superwind can get started, C ignites in the degenerate core.

b) This ignition sets up a runaway thermonuclear reaction as a result of the degeneracy.

c) Unlike the He-flash, this **carbon detonation** completely destroys the star in a **supernova** explosion.

Figure VII–2: Heating and cooling rates versus temperature. Dashed curves give $\Gamma - \Lambda_R$ for three stellar input spectra (T_* denotes the spectral temperature), and $\tau_\circ$ is the optical depth of the medium at the ionization limit.

Figure VII–3: Evolutionary track of a solar mass main sequence star.

d) Such supernovae are sometimes called (which will become apparent at the end of this section of the notes) **Type $\mathbf{I\frac{1}{2}}$ supernovae**.

e) The supernovae remnant *Cassiopeia A* may have been produced by such an explosion since we have not detected any object at the center of this remnant (see a discussion of supernova remnants below).

f) Figure 13.4 of your textbook gives details of an evolutionary model of a 5 $M_\odot$ star as calculated by Iben in 1967. Above the "tip" of the arrow in the upper-right corner of this H-R Diagram is the location of the star when carbon detonation occurs.

7. $\boldsymbol{M > 8M_\odot}$: These stars burn elements up to iron (Fe) in their cores. After Fe is formed in the core, no further energy can be obtained from thermonuclear reactions. As a result, the collapse of the core cannot be halted by the onset of further thermonuclear reactions. There are two possible outcomes for the core depending upon the final core's mass as explained below.

a) Stellar evolution for these stars is similar as the evolution of the lower mass stars, except ^{12}C ignites gradually in non-degenerate gas.

b) As described in §IV.D.6, heavier and heavier elements are created in turn as the core goes through a series of contraction-burning episodes (see the table on page IV-42 in the notes and Fig. 13.14 on page 511 in the textbook).

c) The last stage of core thermonuclear burning is *silicon burning*. Si-burning primary makes the *iron-peak* elements: ^{54}Fe, ^{56}Fe, and ^{56}Ni.

d) Any further thermonuclear reactions beyond Fe are endothermic, hence will take energy away from the core instead of producing it $\Longrightarrow$ silicon burning produces and *iron core*.

e) While this is going on, strong stellar winds cause a large mass-loss rate while these stars are going through their thermonuclear cycles (*i.e.*, $10^{-6} \lesssim \dot{M} \lesssim 10^{-3} M_\odot/\mathrm{yr}$).

f) For each successive stage of thermonuclear burning, the star's evolution proceeds at a quicker and quicker rate: For a 20 $M_\odot$ star, H-burning takes 10^7 years, He burning requires 10^6 years, C burning takes 300 years, O burning takes 200 days, and Si burning is completed in only 2 days!

g) Very high temperatures are now present in the Fe core, so high that the gamma ray photons **photodisintegrate** much of the Fe and Ni that has formed via the following reactions:

$$\begin{aligned}
^{54}\mathrm{Fe} + \gamma &\longrightarrow 13\ ^4\mathrm{He} + 2n \\
^{56}\mathrm{Fe} + \gamma &\longrightarrow 13\ ^4\mathrm{He} + 4n \\
^{56}\mathrm{Ni} + \gamma &\longrightarrow 13\ ^4\mathrm{He} + 2p^+ + 2n \\
^4\mathrm{He} + \gamma &\longrightarrow 2p^+ + 2n\ .
\end{aligned}$$

h) At the same time, this iron core (which can range anywhere from 1.3 $M_\odot$ for a 10 $M_\odot$ ZAMS star to 2.9 $M_\odot$ for a 60 $M_\odot$ ZAMS star) collapses within a fraction of a second to nuclear densities $\Longrightarrow$ electron degeneracy is too weak to halt the collapse.

i) Since the Pauli Exclusion Principle cannot be violated, the following reaction occurs as the photodisintegrations are occurring:

$$e^- + p^+ \longrightarrow n + \nu_e \ .$$

Once nuclear densities are achieved, neutron degeneracy sets in which causes this dense core to *bounce* $\Longrightarrow$ a solid neutron core (called a **neutron star** — see §VIII.B) is left in center surrounded by an expanding shock wave which rips the envelope off of the core in a violent **supernova explosion** (see §VII.D).

j) If the collapsed core (or contracting massive protostar) exceeds 3.0 $M_\odot$, neutron degeneracy cannot support the weight of the core, collapse continues down to zero volume — a **singularity** forms at the center of what is called a **black hole** (see §VIII.D).

8. Figure 13.1 shows a series of evolutionary tracks on the H-R Diagram for different stellar masses. Note that the more massive the star, the quicker it goes through its evolutionary steps.

B. Stellar Pulsations and Mass Loss.

1. The first variable star discovered was *o* Cet in 1596. Astronomers were so surprised by this finding that they renamed the star *Mira* (the wonderful).

a) This was the discovery of the first **long period variable** stars, also called **Mira-type variables** after their prototype *o* Cet.

b) There are a variety of red giant variables stars that have different variability characteristics:

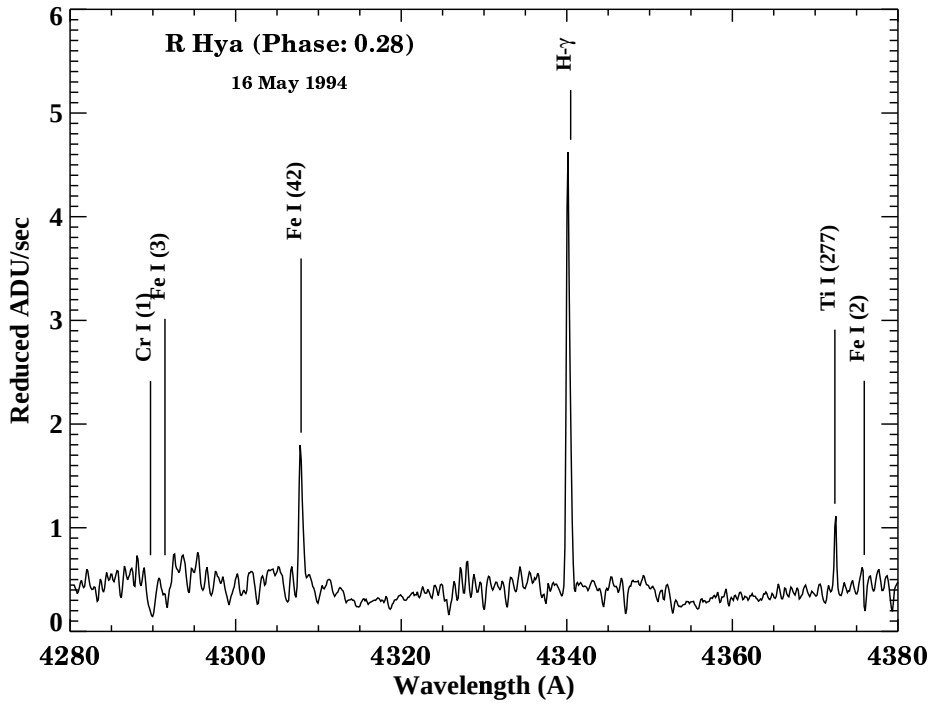

Figure VII–4: Emission lines in the visual spectrum of the Mira-type variable star R Hya.

i) **Mira-type (M) variables**: These variable stars change in brightness on a somewhat periodic time frame anywhere from 150 to 500 days and must have at least a 2.5 change in magnitude from minimum to maximum light. Mira stars are all luminosity class of giants (III). Strong emission lines are seen at various phases of the light curve cycle, primarily from hydrogen Balmer lines and fluoresced Fe I lines in the blue part of the spectrum (see Figure VII-4).

ii) **Semiregular (SR) variables**: These come in 4 subclasses

— *SRa variables*: Giants of spectral class M, C (R & N), and S that are distinguished from the genuine Mira stars by their smaller amplitudes

in light variability, yet in general the periods are maintained to the same extent as in the Mira stars. Emission lines are less frequent.

— *SRb variables*: Giants of spectral class K, M, C, and S. A form of period is evident, but becomes inoperative at times. The changes in brightness are then irregular. Later the period returns, but with altered phase. Emission lines are not seen at visible wavelengths.

— *SRc variables*: Supergiants of spectral classes G8–M6, having almost completely irregular changes in magnitude.

— *SRd variables*: Yellow giants and supergiants of spectral classes F–K. Warmer versions of the SRc variables.

iii) Irregular (L) variables: These are subclassified into 2 groups:

— *Lb variables*: Slow, irregular variables of intermediate and late spectral classes (F to M, C, and S), predominantly giants.

— *Lc variables*: Supergiant versions of the Lb class.

c) All of these types of variable stars are on the asymptotic giant branch of their evolution.

d) The brightness variability is causes by an actual pulsation of the star! The frequency distribution of these variable types as a function of spectral type is shown in Table VII-2. Note that most of the oxygen-rich stars are

Table VII–2: Percentage of stars found in the *General Catalog of Variable Stars* for each spectral class that are in one of the three LPV classes: Mira stars, semiregulars (SR), and irregulars (L).

Spectral Class	**Variability Class** (% in Each Class)		
	Mira	**SR**	**L**
M	46	29	25
S	58	23	19
C (R & N)	20	38	42

Miras and most of the carbon stars are semiregulars and irregular variables.

2. Another type a variable star was discovered in 1784, the **Cepheid variables**, with δ Cephei as the prototype. Later it was recognized that there are 2 different types of Cepheids: "classical" **Cepheids** (or Type I Cepheids), which are higher metal abundance Population I stars, and **W Virginis stars** (or Type II Cepheids), which are low metal abundance Population II stars.

a) Cepheids of both types are luminous supergiant (class Ib) stars that change in brightness by typically a magnitude or less over the period of 1 day to 60 days. The W Vir stars are approximately 2 magnitudes fainter than their δ Cep cousins.

b) These are pulsating stars too. See Fig. 14.5 on page 546 in your textbook for their pulsation characteristics.

c) Cepheids follow a **period-luminosity relationship**, each type has its own unique P-L relationship. The log of the luminosity of the star scales linearly with the pulsational period $\Longrightarrow$ by measuring a Cepheids period, we can deduce its absolute magnitude M_V, then by comparing M_V to its apparent magnitude V, we can deduce its distance via the distance modulus formula (see Eq. II-2).

d) The period-luminosity relation for Type I Cepheids is

$$\log\left(\frac{\langle L\rangle}{L_\odot}\right) = 1.15\,\log P + 2.47\ , \qquad \text{(VII-14)}$$

where $\langle L\rangle$ is the average luminosity of the star and P is the pulsational period in days.

e) Since Cepheids all have approximately the same color, we can rewrite the P-L relation in terms of absolute visual magnitude:

$$\langle M_V\rangle = -2.80\,\log P - 1.43\ , \qquad \text{(VII-15)}$$

where $\langle M_V\rangle$ is the average absolute magnitude of the Cepheid variable.

3. Lower-mass versions of Cepheids exist called **RR Lyrae** type variables, which change in brightness with period shorter than 1 day. These stars are horizontal branch stars, and as such, all have the approximate same luminosity (*e.g.*, $100L_\odot$), hence also can be used as distance indicators.

4. All of these different types of variables pulsate due to their internal structure — they all lie on an **instability strip** on the H-R Diagram (see Fig. 14.6 on page 547 in your textbook).

a) The pulsations are due to the **kappa effect**, kappa for opacity, which results from an ionization zone that lies just beneath the photospheres of these stars.

i) An abundant species such as H or He is ionized just below the photosphere.

ii) Free electrons are very opaque to E/M radiation of all wavelengths due to electron scattering.

iii) There is a net momentum exchange between the photons flowing outward from the interior of the star with these electrons which pushes the electrons (and gas) outward.

iv) As this outermost interior layer expands, it cools to a point where the ionized species once again becomes neutral.

v) The opacity drops as a result and the photon momentum transfer drops by a large amount, lowering the total pressure.

vi) HSE then tries to recover by having these layers settle back to their original positions.

vii) As this layer sinks inward, it heats back up, reionizing the gas which starts the process all over again.

b) Miras pulsate from a hydrogen ionization zone just beneath the surface of the star.

c) Cepheids and RR Lyr's pulsate from a helium ionization zone just beneath the surface (see Fig. 14.12 on page 555 in your textbook).

5. Pulsations can occur at a variety of different modes as described in detail of §14.2 of your textbook. Most of the stars mentioned above pulsate radially or in the **fundamental mode**. It can be shown that the period of oscillation P of a star pulsating in the fundamental mode scales as the reciprocal of the square-root of

the mean density of the star (see Eq. 14.4 on page 549 in your textbook). This scaling law is typically expressed as

$$P\sqrt{\frac{\overline{\rho}}{\overline{\rho}_\odot}} = \text{ constant } = Q \ , \qquad \text{(VII-16)}$$

where $\overline{\rho}$ is the mean density of the star and the *pulsation constant* Q has, in the basic stellar model, a theoretical value of 0.03 days.

6. Some of these stars may oscillate in the **first overtone mode** or show a combination of fundamental mode mixed with first overtone (*e.g.*, the SRs, Ls, and a subclass of Cepheids). If two modes are present in a star, then the periods of these two modes combine to form a *beat* which has a period defined by

$$\frac{1}{P_1} - \frac{1}{P_0} = \frac{1}{P_b}, \qquad \text{(VII-17)}$$

where P_b is the beat period, P_1 is the first overtone period, and P_0 ($P_0 > P_1$) is the fundamental mode period. Indeed, the apparent discontinuities in the SRb stars variability cycle may result from a switch over between fundamental modes and first overtone modes.

7. Sections 14.3 and 14.4 go into the details of **hydrodynamic modeling** of pulsating stars.

8. Hydrodynamic models of Miras have produced a large amount of insight into various peculiarities in the spectra of these stars (which got me interested in these types of stars). In these hydro-calculations, the pulsation of the star results in periodic shock structures which greatly extend the atmosphere with respect to hydrostatic and radiative equilibria models, making semi-empirical models for these stars invalid.

a) In my research during the past decade, there have been three specific spectral characteristics of Mira stars that I have been working on:

i) The H Balmer emission lines are at their peak flux when these stars are at the brightest at visual wavelengths (so-called "phase 0"). Balmer emission lines seen in the ISM (*i.e.*, H II regions), typically display $f(\mathrm{H}\alpha) > f(\mathrm{H}\beta) > f(\mathrm{H}\gamma)$, etc. (*i.e.*, the flux of Hα is greater than Hβ, etc.) — the so-called *Balmer-line decrement*, following their respective oscillator strengths. However, in Miras at phase 0, a *Balmer-line increment* is seen where $f(\mathrm{H}\alpha) < f(\mathrm{H}\beta) < f(\mathrm{H}\gamma)$ with $f(\mathrm{H}\delta)$ being the strongest line, then the lines get weaker and completely disappear as you go to higher-order Balmer lines. Why does this occur?

ii) The peak flux of the Mg II h and k lines in Miras occur around phase 0.3 to 0.4 — a 0.3 to 0.4 phase shift with respect to the peak Balmer-line flux. Why don't they reach peak flux at the same time?

iii) Two strong emission lines from Fe I optical multiplet 42 at 4202 Å and 4306 Å mimic the flux variability of the Mg II lines, reaching their peak flux at the same time as Mg II. Why?

b) Past observers had attributed both the phase lag between Mg II and H Balmer peak flux to overlying absorption (see below), and the Balmer-line increment resulting from overlying TiO absorption. My research has shown that both of these characteristics result from the shocked

nature of the atmospheric structure of these stars (see below).

c) The Bowen (1988, *Astrophysical Journal*, 339, 299) hydrodynamic models (see Fig. 5a & 5b) reproduce many characteristics in the spectra of Mira-type variables. The important findings of both the hydrodynamic calculations and the NLTE radiative transfer calculations for a 5-level hydrogen run include:

i) For non-dusty Miras, the acoustic energy of the shocks produce a region resembling a chromosphere that exists throughout the pulsation cycle (see the region between 2-10 $R_\star$ in Fig. VII-5a). Such a region has been called a *calorisphere* by Willson (1988, in *Pulsations & Mass Loss in Stars*, Kluwer: Dordrect, 285) and a *hydrodynamic chromosphere* by others.

ii) For dusty models, radiation pressure on the dust is an effective energy conduit that prevents a strong chromosphere from forming (see Fig. VII-5b).

iii) The Bowen models produce Balmer-line flux that varies over a pulsation cycle in a manner similar to observed variability.

iv) The famed Balmer-line increment results from radiative transfer effects in a shocked atmosphere and <u>not</u> from overlying TiO absorption.

d) The Balmer-line *increment* is seen in the models <u>without</u> the inclusion of overlying bound-bound opacities in the calculations (see Fig. VII-6) — hence TiO is not needed

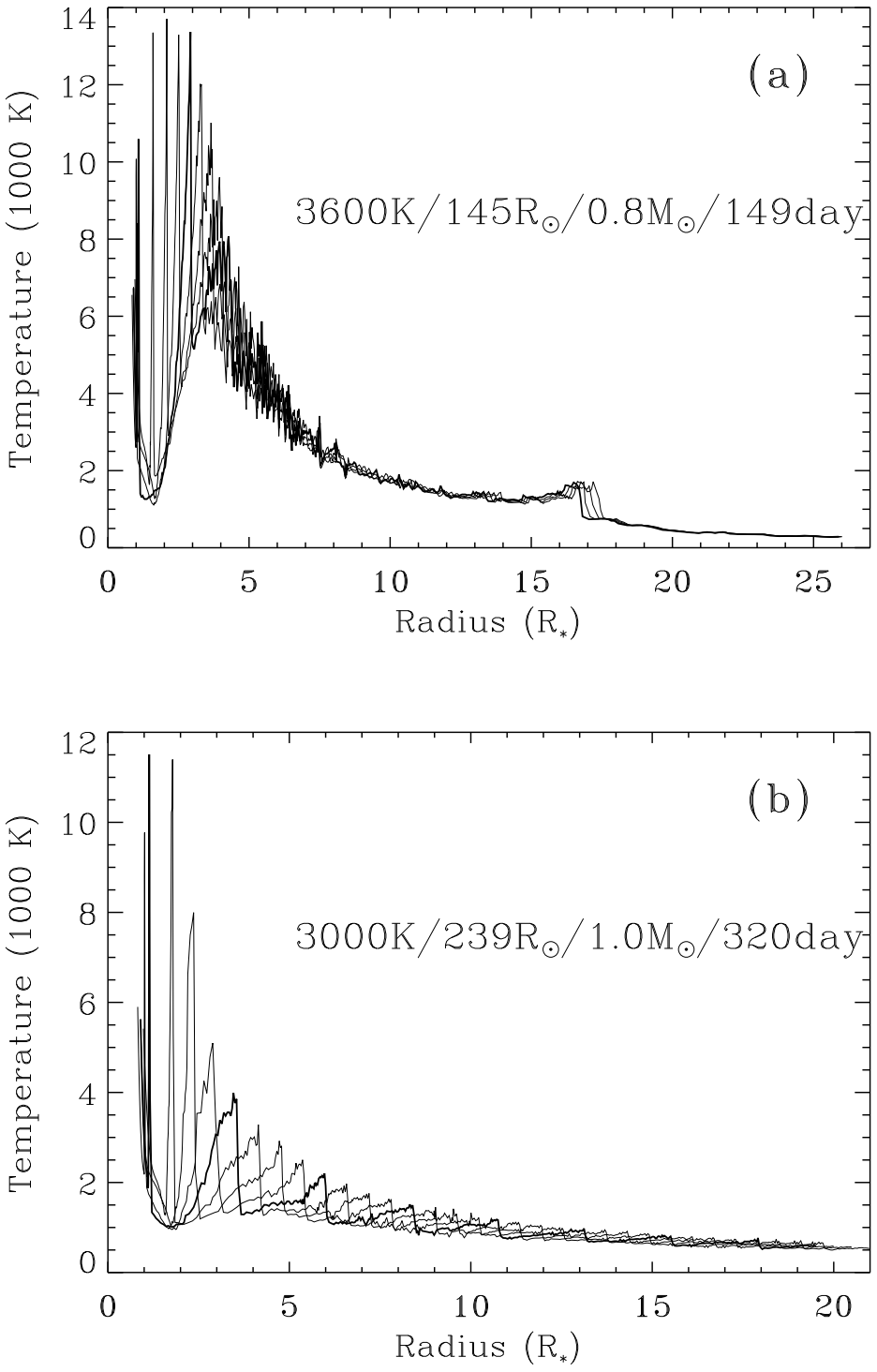

Figure VII–5: Bowen hydrodynamic models for a warmer *non-dusty* Mira (top) and a cooler *dusty* Mira (bottom). Four phases are presented for each hydrodynamic model: Pulsation Phase (PP) 0.00 (photosphere at minimum size just beginning to expand outward, note that Visible Brightness Phase 0.00 occurs at Pulsational Phase 0.85 – the thick line is PP 0.00), PP 0.25, PP 0.50, and PP 0.75. Note how the shocks propagate outward (and weaken) at each subsequent phase.

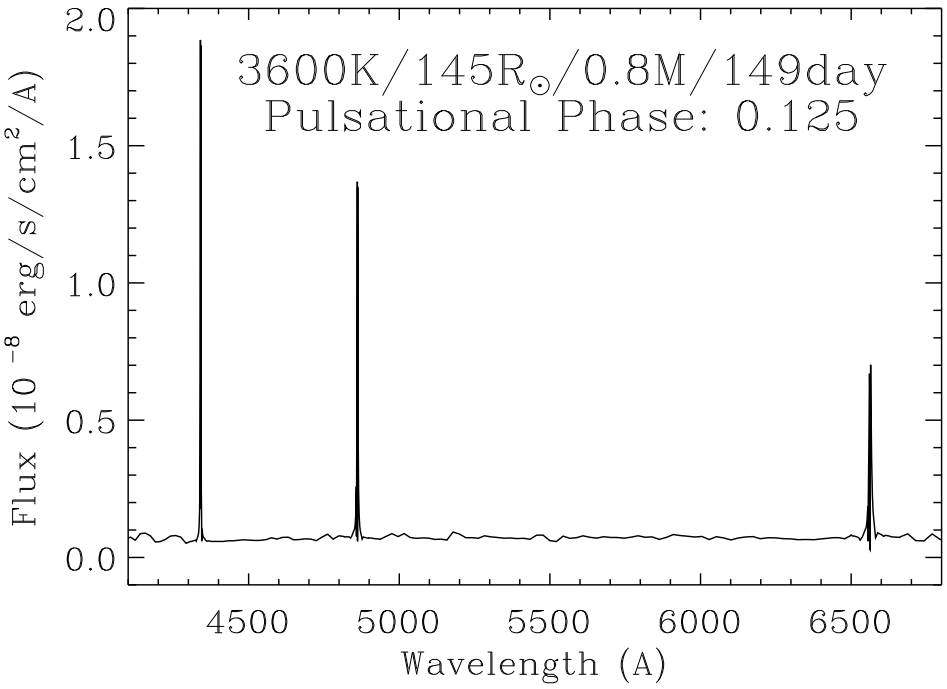

Figure VII–6: A NLTE synthetic spectrum of a 5-level hydrogen run of the non-dusty Mira model made with the radiative transfer code PANDORA. Note how Hγ is stronger than Hα.

to explain this phenomenon. This is the result of two factors in the transfer of radiation in the lines:

i) The optical depth of the line which determines its depth of formation of each line.

ii) The *thermalization* of the line which determines how closely the source function (S_ν) couples to the Planck function (B_ν). Figure VII-7 demonstrates this phenomenon.

- The peak emission of these Balmer lines originates near line-center optical depth of 10^3 (note that the logarithm of the line-center optical depths, $\log \tau_\nu$, are located for each line within the plots of Figure VII-7).

Figure VII–7: The source and Planck functions for the Hα, Hβ, and Hγ transitions in a hydrodynamic model representative of the Mira S Car. Note that the emission seen in Figure VII-6 occurs near line center optical depth 10^3.

- The core of the Hα line, which has the highest optical depth, forms in the 2nd innermost shock in the calorisphere near $\log \tau_\nu = 0$, while the emission wings originate in the temperature minimum region above the innermost shock at phase 0. Note that at this position in the atmosphere, $S_\nu(\mathrm{H}\alpha)$, which is directly related to the number of photons being emitted in this line, is 4 orders of magnitude greater than the Planck function in this temperature minimum region, and is sloping downward from the values found in the innermost shock.

- Meanwhile, the Hβ emission feature forms in the post-shock region of the innermost shock. The higher gas temperature in this zone, as compared to the $\tau = 10^3$ zone of Hα, increases the collisional rates which causes $S_\nu(\mathrm{H}\beta)$ to be more closely coupled to B_ν. Since $S_\nu(\mathrm{H}\beta) > S_\nu(\mathrm{H}\alpha)$ near $\tau = 10^3$ for each line, the flux of Hβ is greater than Hα.

- Hγ, with its even lower oscillator strength, 'sees' a little deeper in the innermost shock, hence samples an even hotter part of the post-shock region. The resulting Hγ emission line is stronger than the Hβ line.

- By extrapolation, the Hδ line samples the hottest part of the innermost shock and the higher order Balmer lines have optical depths low enough that they start to 'see' through the innermost

shock and weaken as compared to Hδ.

e) As the innermost shock continues to propagate outward, it begins to merge into the chromosphere around pulsational phase 0.375. At this point, the Balmer-line emission originate in the chromosphere and they take on the more standard 'chromospheric/ISM' appearance (*i.e.*, $f(\mathrm{H}\alpha) > f(\mathrm{H}\alpha) > f(\mathrm{H}\alpha)$), which agrees with the observations. The lines weaken and vanish shortly thereafter. They reappear around pulsational phase 0.875 when the next strong shocks arises out of the photosphere. This cycle seen in the synthetic spectra mimics the observed variability very well.

f) Another observational characteristic results from a comparison between the UV Mg II h & k lines and the hydrogen Balmer lines $\Longrightarrow$ the peak of the Mg II flux occurs approximately phase 0.3–0.4 after the peak of the Balmer line flux.

i) Once again past observers attributed this to overlying absorption $\Longrightarrow$ obscuration from Mn I and Fe I over the Mg II is at a maximum at phase 0 which hides the flux that is really there.

ii) Luttermoser (2004, *in preparation*) has shown however that the peak flux of the Fe I (42) lines at 4202 Å and 4308 Å, which are fluoresced via the Mg II h & k lines, correspond to the peak flux of the Mg II lines (see Fig. VII-8).

iii) Luttermoser, *et al.* (2004, *in preparation*) have shown through a NLTE analysis that this maximum light phase shift between the H lines and the

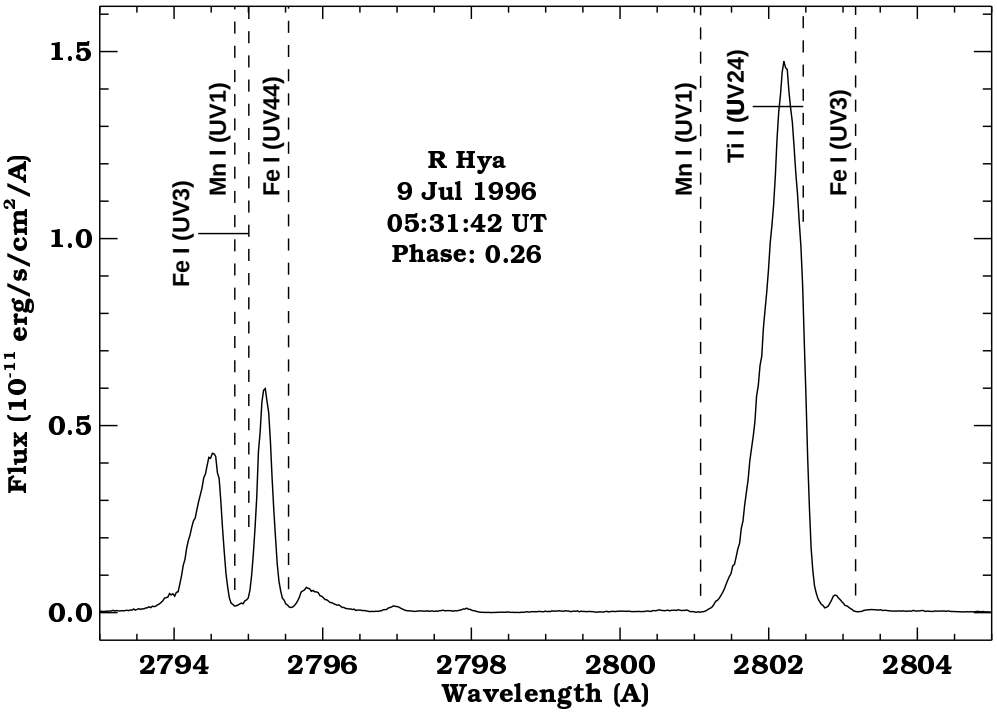

Figure VII–8: The location of strong circumstellar absorbers in the vicinity of Mg II in the spectrum of R Hya.

Mg II lines directly results from the existence of a "hydrodynamic chromosphere".

- In models without this chromosphere, the peak flux of the H and Mg II lines occurred at the same phase since the emission arose from the same depths (*i.e.*, the innermost shock).

- In "calorispheric" models, the Mg II lines form in this chromosphere whereas the H lines form in the innermost shock between the photosphere and chromosphere. The innermost shock enhances the background flux under the Mg II lines which produces absorption lines.

Figure VII–9: The top panel shows the variation of the Balmer line flux as a function of pulsation phase. The bottom panel shows the Mg II lines at the same phases.

- As the shock propagates outward, it merges with the chromosphere, enhancing the temperature and Mg II emission, while the background "continuum" falls away producing Mg II emission features. The shock is now at lower densities, the Balmer line flux is less than it was at earlier phases when the Mg II lines where absorption lines.

- The phase difference between the H line peak flux and the Mg II peak flux in the NLTE calculations is approximately 0.35 in phase which is consistent with the observations (see Figure VII-9).

9. Additional Details of the UV Spectra of AGB Stars.

a) From studying the UV spectra of AGB stars from both IUE and HST, we have learned much about the atmospheric structure of these stars. Figures VII-10 shows a series of high-resolution IUE spectra of a Mira variable over a few pulsation cycles. Note the asymmetries in the lines and the fact that $f(\text{Mg II } h) > f(\text{Mg II } k)$, opposite of their oscillator strengths and their appearance in non-Mira red giants.

b) It is interesting to note the differences and similarities in the UV emission lines for the various spectral and variability classes of red giant stars (see Figure VII-11).

i) R Hya is an M7 IIIe Mira variable with an effective temperature of 2680 ± 70 K when at phase 0.28 which is close to the phase the HST observations were made in Fig. VII-11.

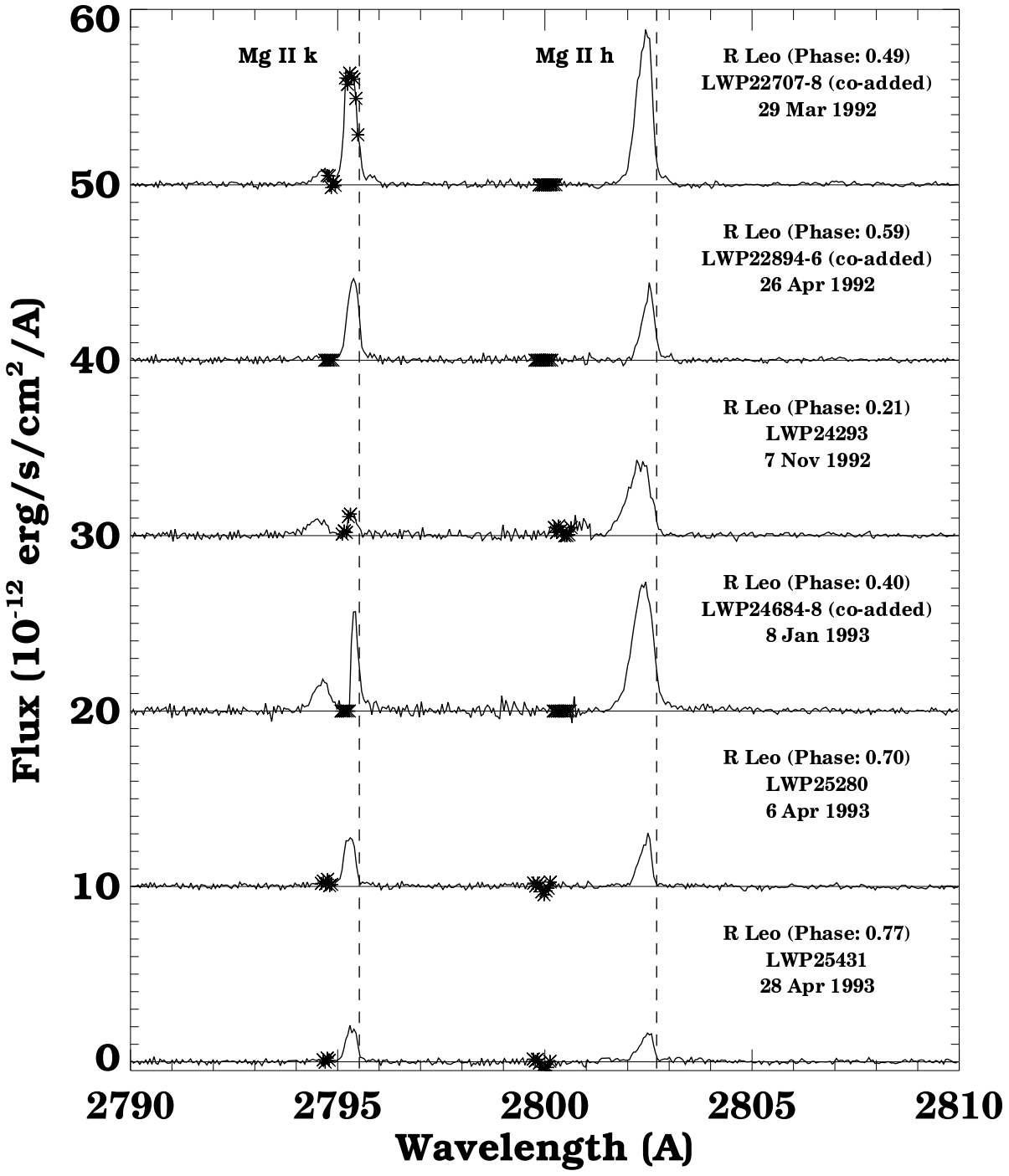

Figure VII–10: A series of high-dispersion IUE spectra of R Leo in the Mg II k & h region taken at various phases over two pulsation cycles. Reseau marks and saturated pixels are marked with '$*$'. All spectra have been shifted by -7.2 km/s to offset the center-of-mass velocity of R Leo. The laboratory wavelengths of Mg II h & k are indicated with a vertical dashed line.

ii) For comparison, HST spectra are displayed for μ Gem, a nonvariable M3 III red giant with an effective temperature of 3587 ± 93 K, and UU Aur, an N2 II cool carbon star at an effective temperature of 2767 ± 25 K. The carbon star is a semiregular (*i.e.*, non-Mira) variable star.

iii) In Mira stars, the Mg II line emission is shifted blueward of the stellar rest velocity, whereas the semiregular, oxygen-rich variable stars and the nonvariable red giants display Mg II emission which is virtually at rest with respect to the stellar photosphere of the star.

iv) Also note that circumstellar absorption is not evident in the earlier red giant star μ Gem (i.e., $F(\mathrm{k})/F(\mathrm{h}) \approx 1.5$) — only the narrow interstellar absorption is seen blue shifted from the self absorption of the upper stellar atmosphere.

v) In terms of UV spectra, the carbon-rich (non-Mira) giants appear more similar to the oxygen-rich Miras – Mg II k & h mutilation by overlying absorption and the appearance of the fluoresced Fe II (UV45) emission line in both spectra (see below).

c) Figure VII-12 shows a comparison of a non-variable red giant (μ Gem, M3 III), non-Mira AGB stars (g Her, M6 III; TX Psc, N0 II), and two Mira AGB stars (R Hya, R Leo) in the C II] spectral region.

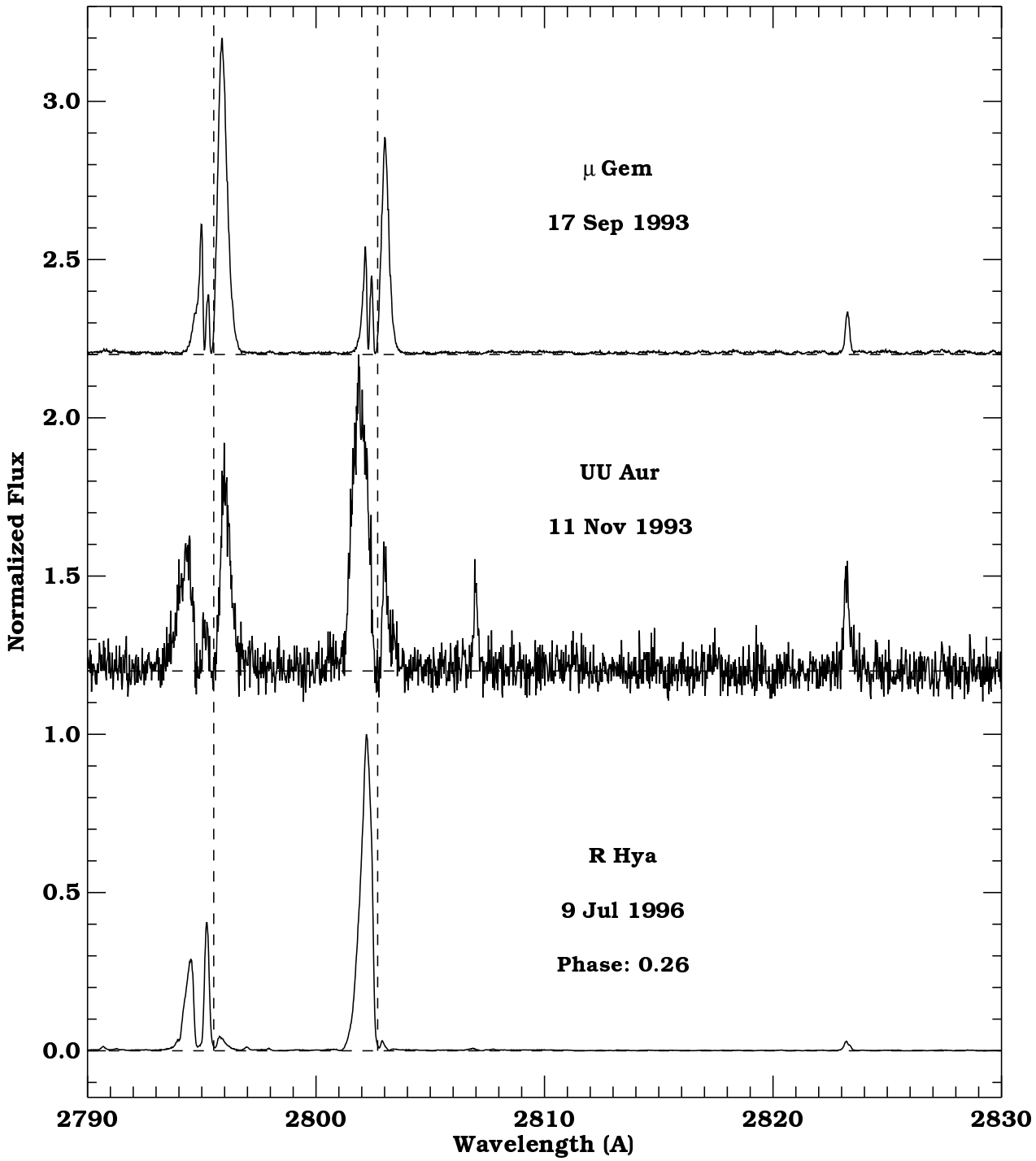

Figure VII–11: Three comparison HST spectra in the Mg II spectral region. Each spectrum has been shifted to the rest frame of the star in question and their peak fluxes have been normalized to unity. Vertical dashed lines represent the laboratory wavelengths of Mg II h & k.

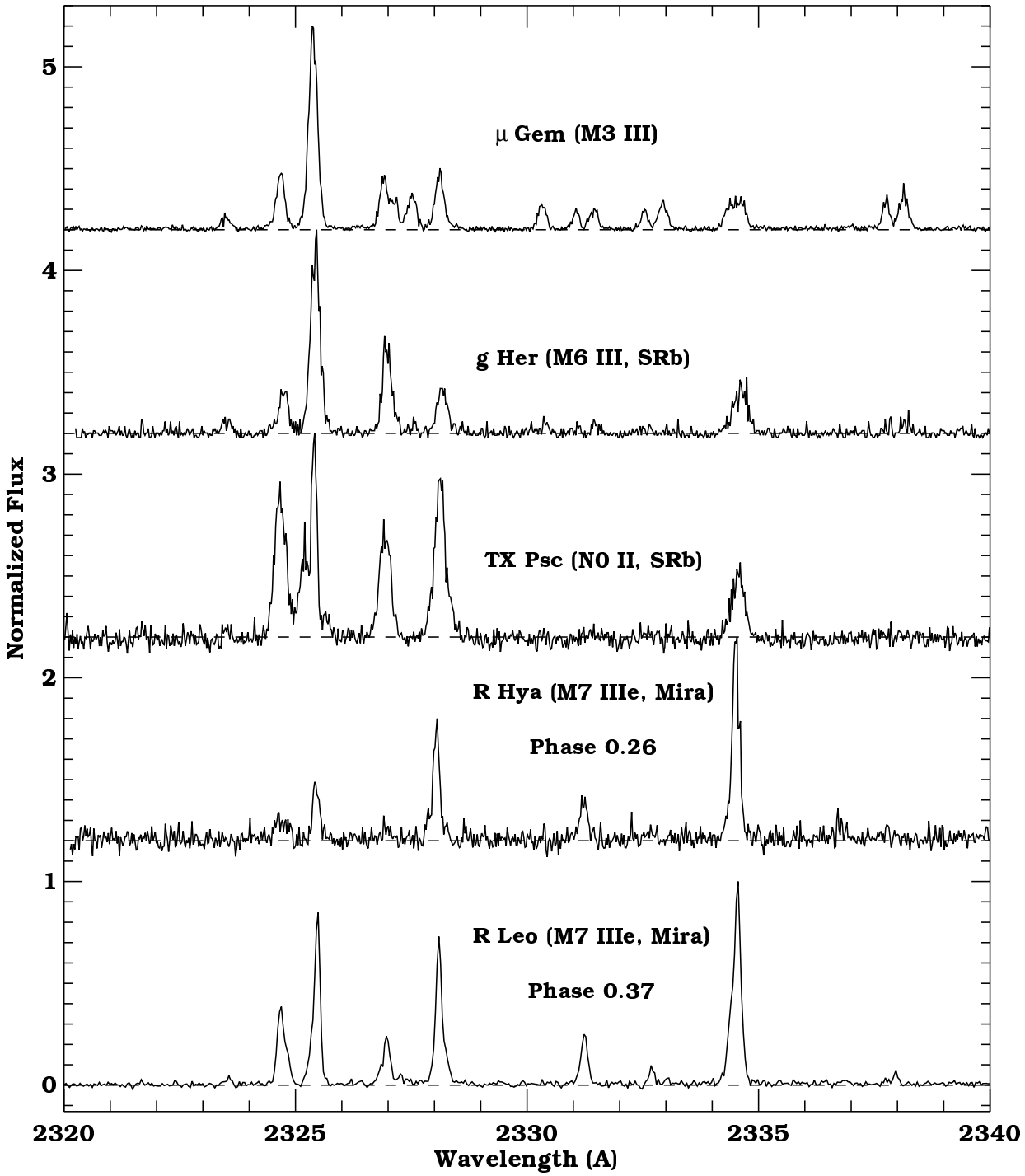

Figure VII–12: A comparison plot of C II] (UV0.01) for five cool giants. Note the dissimilarity between the two Miras with the other two AGB stars. μ Gem represents a non-variable red giant. All spectra are shifted to the stellar rest frame.

i) Although comparisons of the Mg II h & k lines in the two variable types (*i.e.*, semiregular and Mira) of AGB stars show some similarities (see Fig. VII-11), the C II] lines show the emitting region are not identical in these two types of cool stars.

ii) This multiplet gives a fairly accurate measure of electron density n_e in the emitting region (*i.e.*, Lennon *et al.* 1985, *Astrophysical Journal*, **294**, 200), and since the lines in this multiplet are *optically thin* (at least in the non-carbon stars), wavelength shifts are a direct measure of the macroscopic gas velocity of this region of the atmosphere.

iii) NLTE calculations (*e.g.*, Luttermoser & Bowen 1990, 1992) have shown these lines originate in the innermost shock (see Figures VII-5 and VII-7). By monitoring these C II] lines over a pulsation cycle, we can note velocity changes in the innermost shock as it propagates outward.

iv) The relative strengths of these C II] lines give a good clue as to whether the outer atmosphere of a red giant star is in hydrodynamic-type (*i.e.*, shocked) or hydrostatic atmosphere. Figure VII-13 shows the comparison between NLTE radiative transfer calculations for these two different types of atmosphere. The plots in this figure can be compared to the to the observed spectra in Fig. VII-12 — the semiregular carbon stars and the Mira stars appear to be dynamic whereas the semiregular oxygen-rich AGB stars and normal

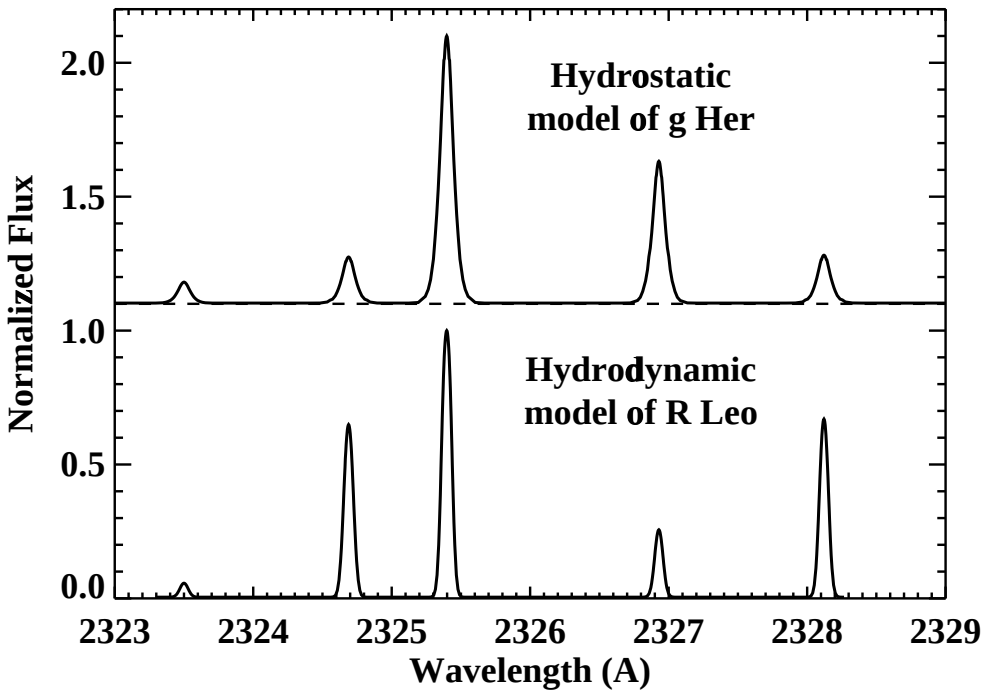

Figure VII–13: PANDORA synthetic spectra at the stellar surface of the C II] (UV0.01) multiplet from a hydrostatic model of g Her (top) and a hydrodynamic model of a Mira (bottom).

red giant stars appear to be in HSE.

d) When high-resolution HST spectra were first taken of carbon stars, the discovery of a fluoresced Fe I (UV45) near 2807 Å was made (IUE didn't have the sensitivity to see this emission feature) as shown in Figure VII-14.

i) This line is pumped by the narrow C II] line at 2325.4 Å through an Fe II (UV13) transition (see Luttermoser 2000, in *The Carbon Star Phenomenon*, Kluwer Academic Press, p.105).

ii) Unfortunately, the obscuration of this carbon line prevents its use in n_e measurements. As a result, only the weaker lines at 2324.7 Å and 2326.9 Å are usable when this fluoresced line is present.

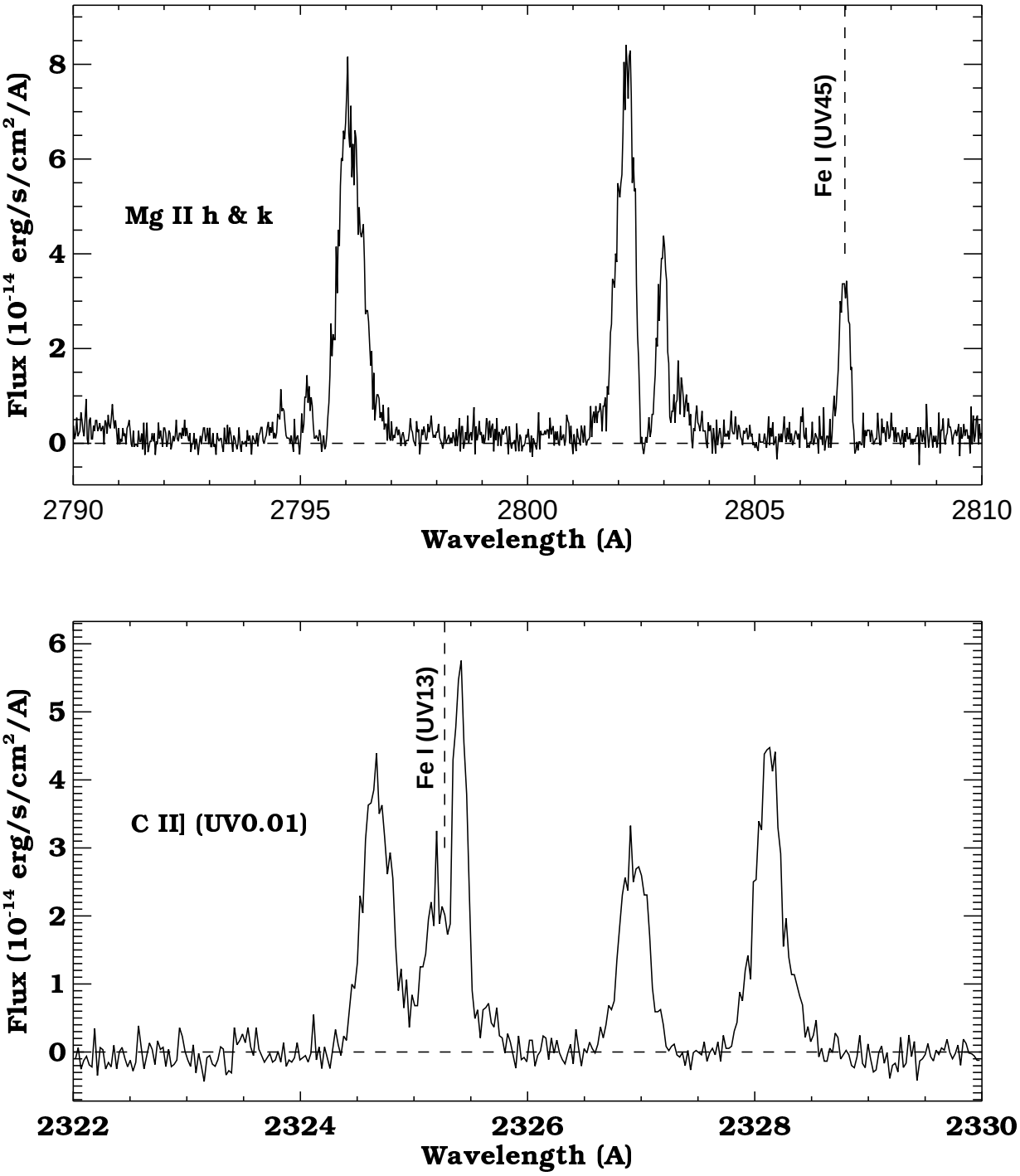

Figure VII–14: HST spectra of TX Psc showing the location of the Fe I (UV45) fluorescent line at 2807 Å and the pumping line in the C II] (UV0.01) multiplet near 2325 Å.

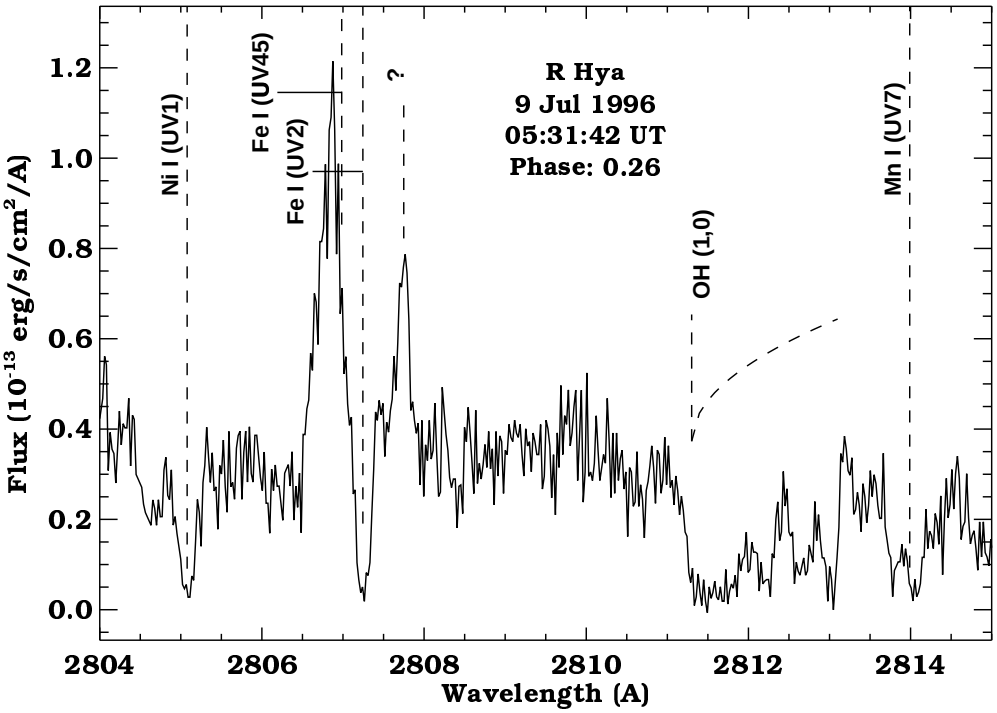

Figure VII–15: As was first noted in the HST spectra of cool carbon stars, oxygen-rich Mira stars also show the fluoresced Fe I (UV45) emission line at 2807.0 Å which is *pumped* by C II]. Prominent absorption features also are identified.

iii) Surprisingly, the fluorescence also is seen in the oxygen-rich Miras as well (see Figure VII-15).

e) One ponders that if the C II] (UV0.01) line can pump Fe I (UV45) in both non-Mira carbon stars and oxygen-rich Mira stars, can the Fe I (42) lines at 4202 Å and 4308 Å be pumped in the semiregular carbon stars as in the Miras, when one considers the large amount of circumstellar absorption over the Mg II lines?

i) From what can be seen in Fig. VII-16, the answer is yes!

ii) These ground-based spectra taken with the McMath telescope on Kitt Peak suggests such fluorescence may be taking place. Figure VII-16

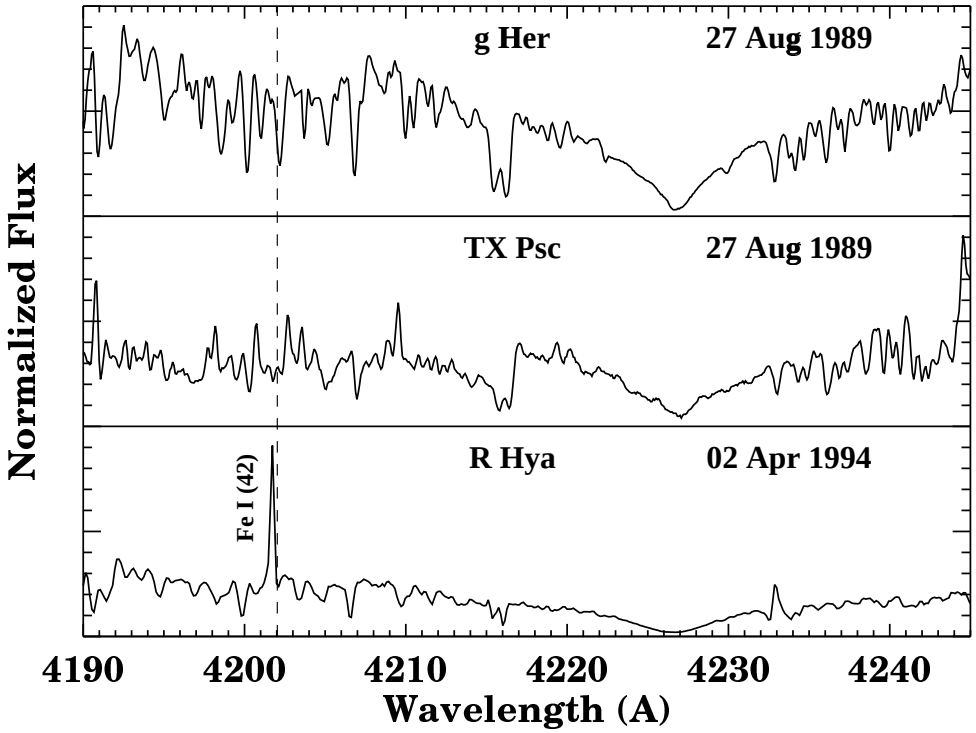

Figure VII–16: A comparison of spectra in the Fe I (42) λ4202 region between TX Psc (N0 II), g Her (M6 III), and the Mira star R Hya (M7 IIIe), where it is in emission. Note that while this feature is a strong absorption line in g Her, it appears to be *filled-in* for TX Psc.

shows a spectrum comparison of TX Psc (N0 II, $T_{\rm eff}$ = 3000 K), the semiregular variable g Her (M6 III, $T_{\rm eff}$ = 3200 K), and the Mira-variable R Hya (M7 IIIe, $T_{\rm eff}$ = 2800 K, Phase 0.2). Where the Fe I (42) line is a strong absorption feature in g Her at 4202 Å, it is a much weaker absorption feature in TX Psc.

iii) This suggests that this absorption line may have been *filled in* by Mg II fluoresced photons in TX Psc. Checking the strength of the other Fe I (42) lines (excluding λ4308, which is also fluoresced by Mg II) in TX Psc shows that the other lines in this multiplet are strong absorption features.

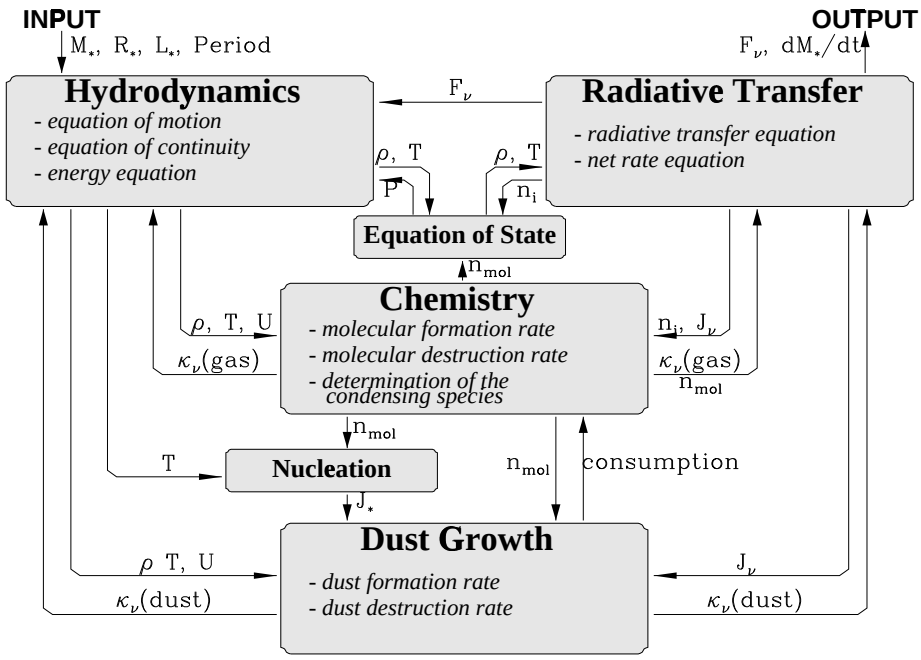

Figure VII–17: A schematic of the basic couplings for self–consistent models of cool variable stars (based on Figure 4 of Sedlmayr, E. 1994, in *Molecules in the Stellar Environment*, ed. U.G. Jørgensen, Berlin: Springer-Verlag, p.163).

iv) This suggests that these two lines are being fluoresced in carbon stars, just not to the same extent that they are in the Mira variables! However, in order to test this suggestion, detailed radiative transfer calculations still need to be carried out.

v) Also note that the broad absorption feature at 4227 Å is the Ca I (2) resonance line and the "double-lined" molecular absorption band at 4216 Å is due to the CH molecule in Fig. VII-16.

10. Figure VII-17 shows the complex logic in determining realistic models of late-type giant and supergiant stars.

a) Recently, computer technology has allowed us to tackle such a formidable problem.

b) The regions in the outer atmospheres of cool giant stars are dominated by nonequilibrium and dynamic effects. The UV spectra that these stars generate originate from these dynamic layers.

c) It is only through comparisons between observations and synthetic spectra that we can probe the atmospheres of these stars, leading to significant improvements to our understanding of the winds of these stars and the chemical enrichment of our galaxy.

C. Stellar Evolution in Binary Star Systems.

1. We will not discuss the kinematics, dynamics or morphology of binary star systems in these course notes (and you will not be tested on these topics). See Chapter 7 for details of these subjects.

2. Instead, here, we will concentrate on stellar evolution in *close* binary star systems where *mass transfer* has a large impact of the evolution of these systems. For binary star systems where the companions are far apart, stellar evolution follows those steps that we have already outlined for isolated stars.

3. Chapter 17 in your textbook by Carroll and Ostlie give the evolutionary details of such systems. We will summarize this section here starting with the gravitational field in a binary star system.

a) By "close," we mean that the separation 'a' of the two stars are at most the diameter of the larger star (*i.e.*, $a \leq 2R_1$, where '1' is the larger of the two stars).

b) Such stars will be tidally (*i.e.*, rotationally) "locked" to each other due to the conservation angular momentum

(see page 683 in the textbook). The *effective* potential energy of such a system is given by

$$U = -G\left(\frac{M_1 m}{s_1} + \frac{M_2 m}{s_2}\right) - \frac{1}{2}m\omega^2 r^2 \ , \qquad \text{(VII-18)}$$

where the M-s are the masses of the two stars in the binary (labeled '1' and '2'), m is a *test* (*i.e.*, negligible) mass in the vicinity of the 2 stars, the s-s are the distances that m is from M_1 and M_2, r is the distance that m is from the center of mass, and ω is the angular velocity of the system (see Figure 17.1 on page 685 in the textbook).

c) For convenience, the effective potential energy can be divided by m to obtain the **effective gravitational potential** Φ (erg/gm),

$$\Phi = -G\left(\frac{M_1}{s_1} + \frac{M_2}{s_2}\right) - \frac{1}{2}\omega^2 r^2 \ . \qquad \text{(VII-19)}$$

i) From the law of cosines, the distances s_1 and s_2 are given by

$$\left.\begin{aligned} s_1^2 &= r_1^2 + r^2 + 2r_1 r\cos\theta \\ s_2^2 &= r_2^2 + r^2 - 2r_2 r\cos\theta \ , \end{aligned}\right\} \qquad \text{(VII-20)}$$

where r_1 is the distance that mass M_1 is from the center of mass, r_2 is the distance that mass M_2 is from the center of mass, and θ is the angle the r vector makes with respect to the r_2 vector (see Fig. 17.1).

ii) The angular frequency (= angular velocity) of the system can be calculated from Kepler's third law since close binary stars will always orbit the center of mass in circular orbits:

$$\omega^2 = \left(\frac{2\pi}{P}\right)^2 = \frac{G(M_1 + M_2)}{a^3} \ . \qquad \text{(VII-21)}$$

d) Plotting this potential in an x-y plane (see Figs. 17.2 and 17.3 in the textbook) shows that 5 points exist where the force on the test mass equals zero,

$$\vec{F} = -\vec{\nabla}U = -m\vec{\nabla}\Phi = 0 \ . \qquad \text{(VII-22)}$$

These points are called **Lagrangian points**:

i) $\boldsymbol{L_1}$: The zero-force point that lies between the two masses M_1 and $M_2 \Longrightarrow$ the *inner Lagrangian point*. The distances that L_1 is from M_1 and M_2 are

$$\ell_1 = a\left[0.500 - 0.227\log\left(\frac{M_2}{M_1}\right)\right] \qquad \text{(VII-23)}$$

$$\ell_2 = a\left[0.500 + 0.227\log\left(\frac{M_2}{M_1}\right)\right] . \qquad \text{(VII-24)}$$

ii) $\boldsymbol{L_2}$: The zero-force point that lies on the far side of M_2 (the smaller mass).

iii) $\boldsymbol{L_3}$: The zero-force point that lies on the far side of M_1 (the larger mass).

iv) $\boldsymbol{L_4}$: The zero-force point that lies in the orbit of M_2 (the smaller mass), 60° forward from M_2 at a distance r_2 from the center of mass.

v) $\boldsymbol{L_5}$: The zero-force point that lies in the orbit of M_2 (the smaller mass), 60° behind M_2 at a distance r_2 from the center of mass.

vi) The first 3 Langrangian points (*i.e.*, L_1, L_2, & L_3) are *unstable* (*i.e.*, if moved away from one of these points, the test mass would continue to move away from that point) since $\nabla\Phi < 0$.

vii) The last 2 Langrangian points (*i.e.*, L_4 & L_5) are *stable* (*i.e.*, if moved away from one of these points, the test mass would move back to that point) since $\nabla\Phi > 0$. In the case of Jupiter's orbit about the Sun, the *Trojan asteroids* are found at Jupiter's L_4 and L_5 Lagrangian points.

e) The equipotential surface of these two stars that just connects with L_1 (it has a teardrop shape as shown in Fig. 17.3) is called the **Roche lobe** (see Fig. 17.4).

i) If the 2 stars in the binary are too small to fill their Roche lobe, they are said to be in a **detached binary** system.

ii) If one star fills it Roche lobe (and the other has not), the system is said the be a **semidetached binary**. In such a system, the star that has filled it's Roche lobe is called the *secondary* of the binary star independent of what its mass might be with respect to the *primary* star.

iii) If both stars fill their Roche lobe, the system is called a **contact binary**.

f) There are many types of close binary star systems. Your textbook lists some of the better known such systems on pages 707-710. Study these various binary types on your own.

4. The **mass transfer rate** in a semidetached system can be determined with the mass flux equation

$$\dot{M} = \rho v A \ , \qquad \text{(VII-25)}$$

where A is the cross-sectional area of the "tube" of material of density ρ flowing at velocity v through the L_1 Lagrangian point in the system. From a little geometry and thermodynamics, it can be shown that

$$\dot{M} \approx \pi R d \rho \sqrt{\frac{3 k_{\rm B} T}{\mu m_{\rm H}}} \ , \qquad \text{(VII-26)}$$

a) As material flows through L_1, M_1 loses mass and M_2 gains mass through the process of **accretion**.

b) This mass transfer can slow the speed of the evolutionary "steps" of the M_1 star (if it is fast enough) and increase the speed of the evolutionary "steps" of the M_2 star.

c) Nuclear processed material can then be transferred to the companion (this is how dwarf S stars and dwarf carbon stars are made).

d) Sooner or later, one of the stars will reach the final stage of its thermonuclear lifetime.

e) If such a star is massive enough, it will supernovae as described in §§A.6 and A.7 of this section of the notes. Depending upon the distance of the two stars, three possible outcomes will take place of the "secondary" star:

i) It will be ejected from the system.

ii) It will be completely disrupted by the shock wave of the supernova.

iii) It will experience mass loss (perhaps a substantial amount) by the shock and radiation pressure of the blast.

f) If the star in it final thermonuclear stages has too small a mass to supernova, it will lose its envelope through the creation of a planetary nebula (which will have little impact on the secondary) forming a white dwarf star in orbit about the secondary star of the system.

i) As this secondary star starts to fill its Roche lobe through stellar evolution, it will begin to dump material onto the white dwarf.

ii) Since the two stars are in orbit about each other, the material misses the white dwarf on *first pass* and goes into orbit about the white dwarf forming an **accretion disk** (see §17.2 on page 692 in your textbook).

iii) Viscosity (*i.e.*, internal fluid friction) causes the material in the disk to slowly spiral in towards the white dwarf. As the gas falls into the potential well, its orbital speed increases, which increases the viscosity, which increases the thermal energy of the gas in the disk $\Longrightarrow$ the inner portion of the disk is much hotter than the outer portion.

iv) The bulk of the light that is emitted in such a system comes from the inner region of the accretion disk and not from the "normal" star nor the white dwarf.

g) Instabilities can arise in the disk which can result in a rapid increase of the mass flow down through the disk, which in turn, causes a rapid increase in the light output of the system. Such a binary is called a **cataclysmic**

variable and can go through numerous (though not necessarily periodic) episodes of rapid brightenings. The most energetic of the cataclysmic variables are called **dwarf novae**. Such systems usually have a mass-transfer rate of $10^{-11} - 10^{-10} M_\odot$/yr during the long quiescent intervals.

5. When the mass-transfer rate from the normal star exceeds 10^{-8} $M_\odot$/yr, material accumulates fast enough on the inner edge of the accretion disk and the surface of the white dwarf for a thermonuclear runaway to occur.

a) When about 10^{-5} to $10^{-4} M_\odot$ of hydrogen has accumulated, the temperature of this gas reaches a few million Kelvins.

b) A shell of burning hydrogen develops using the CNO cycle (from carbon left over from the stellar evolution of the primary).

c) Due to the high pressures caused by the intense gravitational field on the surface of the white dwarf, the gas is degenerate.

d) This results in a thermonuclear runaway to occur. The result is a runaway thermonuclear reaction, with temperatures reaching 10^8 K before the electrons lose their degeneracy.

e) When the luminosity exceeds the Eddington limit (see Equations V-10 and V-11) of about 10^{38} erg/s, the radiation pressure can lift the accreted material and expel it into space.

f) Such an outburst is called a **classical nova** or just **nova**. They all reach the approximate same maximum brightness of $M_V \approx -4.5$.

i) A *fast nova* takes a few weeks to dim by 2 magnitudes after reaching maximum brightness.

ii) A *slow nova* may take nearly 100 days to decline by the same amount from maximum.

iii) The fast and the slow speed classes of novae are probably due to variations in the mass of the white dwarf and in the degree of CNO enrichment of the hydrogen surface layer.

iv) It takes about 10^4 to 10^5 years to accumulate enough material for another runaway to occur. Since this is short in comparison to stellar evolutionary time scales, such systems can go through numerous nova episodes.

6. If the mass-transfer rate can get as high as $10^{-6} M_\odot$/yr or greater, the white dwarfs mass may build fast enough for its mass to exceed the **Chandrasekhar limit** of 1.4 $M_\odot$ (see §VIII.A).

a) The white dwarf collapses since the degenerate electron pressure is insufficient to support that weight of this burnt-out core.

b) This sets up a runaway thermonuclear event in the core of the white dwarf which completely destroys the white dwarf as was the case in the carbon detonation of the 4-8 $M_\odot$ main sequence stars (see page VII-13 of these course notes).

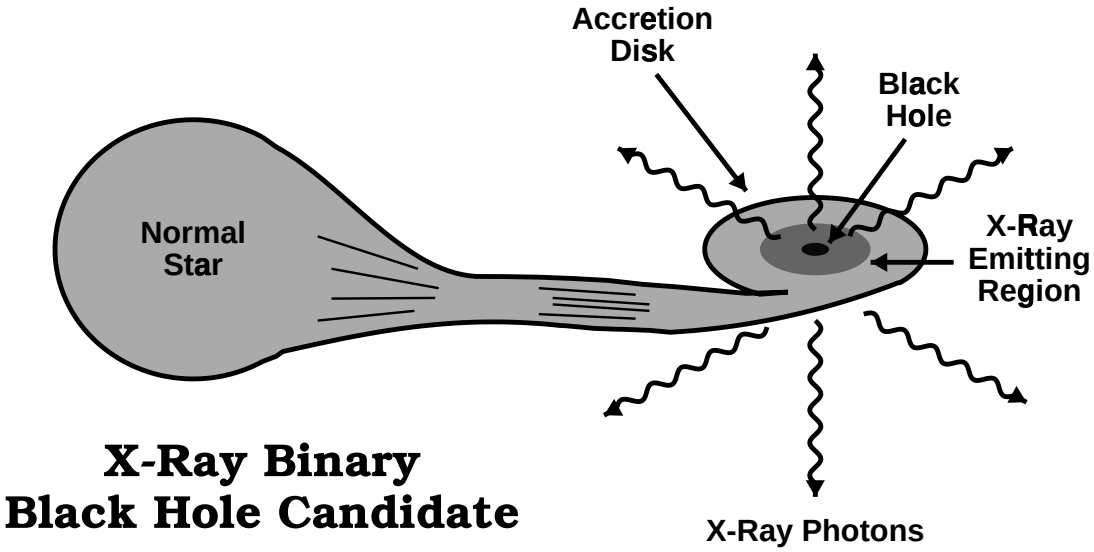

Figure VII–18: A model of a binary star system containing a black hole.

c) Such supernova (see §VII.D) are called **Type Ia Supernovae**.

7. Besides white dwarfs in a close binary system, the primary also can be a neutron star or black hole (see next section). Indeed, **X-ray binary systems** are suspected to contain one of these two objects $\Longrightarrow$ the X-rays are emitted from the extremely hot (perhaps a high as a billion Kelvins!) inner portion of the accretion disk as shown in Figure VII-18.

D. Supernovae.

1. Supernovae are classified based primarily upon their spectra and their light curves (*i.e.*, how brightness changes with time). We have already discussed a few different types. We now present the complete supernova classification scheme. The primary classification is based upon the appearance of hydrogen Balmer lines.

a) **Type I** supernovae do <u>not</u> show hydrogen Balmer lines and reach a maximum brightness of $M_V \approx -19$. They are classified into 3 subclasses:

i) **Type Ia** supernovae display a strong Si II line at 6150 Å. These are white dwarfs in close binary star systems that exceed the Chandrasekhar limit and explode from a runaway thermonuclear reaction in the carbon-oxygen core of the white dwarf. These types of supernovae are seen in both elliptical galaxies and throughout spiral galaxies.

ii) **Type Ib** supernovae display strong helium lines. These tyeps of supernovae are only seen in the arms of spiral galaxies near star forming regions. Hence, this implied that short-lived massive stars in binary systems are probably involved. These explosions are similar to that of a Type II supernova, only in a binary star system where the outer H envelope has been transferred to the secondary star in the system before the Fe-core bounce.

iii) **Type Ic** supernovae display weak helium lines and no Si II is seen. Other than this, they are observed in the same location in galaxies as Type Ib. These types of supernovae are likely the same as Type Ib, except the helium-shell has been transferred to the companion in addition to the hydrogen envelope.

b) **Type I$\frac{1}{2}$** supernovae display weak hydrogen lines. These are isolated stars of main sequence mass of the range 4-8 $M_\odot$ where carbon detonates in a degenerate core and completely disrupts the star. Hydrogen lines are weak due to earlier mass loss on the AGB which results in a lower mass hydrogen envelope in comparisons to the Type II supernovae.

c) **Type II** supernovae display strong hydrogen lines and reach a maximum brightness of $M_V \approx -17$. These supernovae result from the explosion of an isolated star due to an Fe-core bounce. They are classified into 2 subclasses base upon the shape of their light curve (see Figure 13.16 on page 516 in the textbook).

i) **Type II-L** supernovae display a linear decline in their light curves after maximum emission is reached.

ii) **Type II-P** supernovae display a plateau in the light curve between 30 and 80 days after maximum light. This plateau results from additional light generated from the radioactive decay of the large amounts of ^{56}Ni that was created in the explosion. These supernova are likely more massive than the Type II-L supernova which accounts for the larger amounts of this radioactive isotope of nickel in these explosions.

2. During the explosion, material is ejected off of the core at very high velocities. Fast moving free neutrons given off by all of the nucleosynthesis occurring in the outward moving shock interact with nuclei in the envelope to make different chemical elements $\Longrightarrow$ such nuclear reactions are called **rapid neutron capture** or the **r-process**.

a) Most of the heavy elements on the periodic table are made from this r-processed material during supernovae (the iron in your car was made in a supernova, whereas the carbon in your DNA was made via the triple-α process in a now extinct AGB star!).

Figure VII–19: Radio spectrum of the supernova remnant Cassiopeia A.

b) Additional nuclear reactions can occur too from slow moving neutrons, the so-called **slow neutron capture** or **s-process**. This process also occurs during normal thermonuclear burning while a star is on the main sequence, RGB, RGC (or horizontal branch), and AGB.

3. Supernovae send the envelope of the star, with its nuclear-processed material, out into the ISM at supersonic speed. As this material collides with the ISM material, shocks form which ionizes the gas and produces enough opacity to "light up" the gas $\Longrightarrow$ a **supernova remnant** is seen. Supernova remnants emit light at virtually all wavelengths. They are especially bright at radio wavelengths (see Figure VII-19). But what gives rise to this light?

a) Can this emission be due to *thermal radiation*?

i) If the spectrum results from thermal radiation (*i.e.*, the gas is hot), then the equation of transfer

can be written as

$$I_\nu = B_\nu \left(1 - e^{-\tau_\nu}\right) \ , \qquad \text{(VII-27)}$$

where I_ν is the observed intensity, B_ν is the Planck function expressed in frequency units, and τ_ν is the optical depth (see Eq. I-18) of the gas.

ii) The Planck function is just the radiant intensity of an ideal blackbody. At radio wavelengths, $h\nu \ll k_{\rm B}T$ and we can approximate the Planck function (as shown in Eq. I-14) by doing a Taylor expansion of the exponent in the denominator giving

$$B_\nu(T) \approx \frac{2h\nu^3/c^2}{1 + h\nu/k_{\rm B}T - 1} = \frac{2k_{\rm B}T\nu^2}{c^2} \ , \quad \text{(VII-28)}$$

which is called the **Rayleigh-Jeans Law**. As can be seen, this law is just an approximation to the Planck function and is only valid when $h\nu \ll k_{\rm B}T$ (*i.e.*, at radio wavelengths).

iii) If the optical depth is large (*i.e.*, $\tau_\nu \gg 1$), the exponential term in Eq. (VII-27) is negligible and the intensity can be written as

$$I_\nu = B_\nu(T) = \frac{2k_{\rm B}T\nu^2}{c^2} \ . \qquad \text{(VII-29)}$$

iv) If the optical depth is small (*i.e.*, $\tau_\nu \ll 1$), we can Taylor expand the exponential term in Eq. (VII-27) to give

$$I_\nu = B_\nu \tau_\nu \ . \qquad \text{(VII-30)}$$

v) However as can be seen in Figure VII-19, the spectra of supernova remnants show that the intensity I_ν scales as a *negative* power law in frequency and not a positive power law, hence the emission from supernova remnants cannot be thermal radiation. This power law has the following form:

$$I_\nu \propto \nu^{-\alpha}, \qquad \text{(VII-31)}$$

where α scales between 0.5 and 1.0 $\Longrightarrow$ the radio intensity reaches large values at low frequencies!

b) In 1950, H. Alfvén, N. Herlofson, and K.O. Kiepenheuer were the first astrophysicists to understand this **non-thermal emission**.

i) Electrons moving in an external magnetic field H will emit radiation at a characteristic frequency

$$\nu_{\rm H} = \frac{eH}{2\pi m_e c}, \qquad \text{(VII-32)}$$

where e is the electron charge and m_e its mass (in cgs units). This is the frequency at which the electron gyrates about magnetic lines of force perpendicular to its direction of travel.

ii) If $E > m_e c^2$, the electron is said to be relativistic. When this happens, the electron radiates with a continuous spectrum of energies instead of one definite frequency. This radiation will reach its maximum intensity at

$$\nu_{\rm max} = \frac{eH}{4\pi m_e c}\left(\frac{E}{m_e c^2}\right)^2 \qquad \text{(VII-33)}$$

where $\nu_{\rm max}$ is sometimes called the *critical frequency* ν_c $\Longrightarrow$ such emission is called **synchrotron radiation**.

iii) Nearly all the radiation is concentrated within a cone whose axis coincided with the direction of the electron's instantaneous velocity and whose vertex angle is

$$\theta = \frac{m_e c^2}{E} \ , \qquad \text{(VII-34)}$$

as shown in Fig. 15.17 on page 615 in the textbook $\Longrightarrow$ the light is said to be **polarized**.

iv) The volume emissivity (in erg/s/Hz/cm^3/sr) of the relativistic radiation of a group of electrons is

$$\eta_\nu = \int P_\nu N(E)\, dE \ , \qquad \text{(VII-35)}$$

where P_ν is the total power radiated per unit frequency interval by one electron, and $N(E)\, dE$ is the number of electrons per unit volume per unit solid angle along the line of sight which are moving in the direction of the observer and whose energies lie in the range E and $E + dE$.

v) Most of the cosmic rays (the majority being protons and α-particles traveling at relativistic velocities) that are observed interacting with the Earth's atmosphere are assumed to have originated in supernova explosions.

vi) These observed cosmic rays have a power-law spectrum, and because the spectra of many radio sources (including supernova remnants) follow power laws, it is often assumed that the enrgy distribution of electrons synchronously radiating in a supernova remnant have the following energy

distribution:

$$N(E)\,dE = K\,E^{-\gamma}\,dE\ , \qquad \text{(VII-36)}$$

where the kinetic energy E exceeds the rest mass of the electrons (*i.e.*, $E > m_e c^2$), γ is the absolute magnitude of the slope of the spectrum plotted in log-space, and K is a constant deduced from a given spectrum. As such, both γ and K are empirical constants based upon observed spectra.

vii) With Equations VII-35 and VII-36 (and a whole alot of algebra when the power integral, which is the integral of a Bessel function, is evaluated), we can write the intensity of synchrotron radiation as

$$\begin{aligned} I_\nu = \ell\,\eta_\nu &= K\,\ell\,u(\gamma)\,\frac{\sqrt{3}}{8\pi}\,\frac{e^3}{m_e c^2}\left[\frac{3e}{4\pi m_e^3 c^5}\right]^{(\gamma+1)/2} \times \\ &\quad H^{(\gamma+1)/2}\,\nu^{-(\gamma-1)/2} \qquad \text{(VII-37)} \\ &\approx 9.33\times10^{-24}\,u(\gamma)\,K\,\ell\,H^{(\gamma+1)/2} \times \\ &\quad \left(\frac{6.26\times10^{18}}{\nu}\right)^{(\gamma-1)/2} \text{erg/s/cm}^2\text{/Hz/sr}, \end{aligned}$$

where H is the magnetic field strength measured in gauss, ℓ denotes the length along the line of sight of the region in which the relativistic electrons are moving (in cm), K and γ are the constants defined in Eq. (VII-36), and $u(\gamma)$ is a unitless numerical factor of order unity (and slowly varying with respect to γ) given by

$$u(\gamma) = 2^{(\gamma-3)/2}\,\frac{\gamma+7/3}{\gamma+1}\,\Gamma\left(\frac{3\gamma-1}{12}\right)\,\Gamma\left(\frac{3\gamma+7}{12}\right) \qquad \text{(VII-38)}$$

when $\gamma > 1/3$ (which it is as deduced from observed spectra). In Eq. (VII-38), Γ represents the gamma function.

viii) As can be seen, such a distribution of electrons produces a spectrum that reproduces what is seen in nature. By comparing Eq. (VII-37) to Eq. (VII-31), we immediately see that

$$\alpha = \frac{\gamma - 1}{2} \ . \qquad \text{(VII-39)}$$

ix) For Cassiopeia A, $\alpha = 0.8$ from the intensity-spectral observations which gives $\gamma = 2.6$ for the relativistic electron number density as a function of energy — a typical value for cosmic rays, hence consistent for the assumption we have made in the functional form of Eq. (VII-36).